The Vibrational Spectrum of the Secondary Electron Acceptor, A_1, in Photosystem I

Shana L. Bender,[‡] James M. Keough,[‡] Scott E. Boesch,[†] Ralph A. Wheeler,[†] and Bridgette A. Barry*,[‡]

Department of Chemistry and Biochemistry and the Petit Institute for Bioengineering and Bioscience, Georgia Institute of Technology, Atlanta, Georgia 30332, and Department of Chemistry and Biochemistry, University of Oklahoma, Norman, Oklahoma 73019

Received: September 18, 2007; In Final Form: December 17, 2007

Photosystem I (PSI) is a multisubunit protein complex which carries out light-induced, transmembrane charge separation in oxygenic photosynthesis. In PSI, the electron-transfer pathway consists of chlorophyll and phylloquinone molecules, as well as iron−sulfur clusters. There are two phylloquinone molecules, which are located in structurally symmetric positions in the reaction center. It has been proposed that both phylloquinone molecules are active as the A_1 secondary electron acceptor in bidirectional electron-transfer reactions. The PSI A_1 acceptors are of interest because they have the lowest reduction potential of any quinone found in nature. In this work using light-induced FT-IR spectroscopy, isotope-edited spectra are presented, which attribute vibrational bands to the carbonyl stretching vibrations of A_1 and A_1^- and the quinoid ring stretching vibration of A_1. Bands are assigned by comparison with hybrid Hartee−Fock density functional calculations, which predict vibrational frequencies, amplitudes, and isotope shifts for the phylloquinone singlet and radical anion states. The results are consistent with an environmental interaction increasing the frequency of the singlet CO vibration and decreasing the frequency of the anion radical CO vibration, relative to model compounds. This environmental interaction may be the asymmetric hydrogen bond to A_1/A_1^-, electrostatic interactions with charged amino acid side chains, or a pi−pi interaction with the indole ring of a nearby tryptophan. Such differential effects on the structure of A_1 and A_1^- may be associated with a destabilization of the anion radical. These studies give novel information concerning the effect of the protein matrix on the PSI electron-transfer cofactor.

Introduction

In oxygenic photosynthesis, photosystem I carries out the light-driven oxidation of plastocyanin and the reduction of ferredoxin. These reactions lead to a charge separation across the thylakoid membrane. Electron transfer is initiated by photoexcitation of the photosystem I primary chlorophyll donor, which reduces the primary acceptor, A_0, a chl *a* monomer.[1] The resulting positive charge resides on P_{700}, a heterodimeric chlorophyll, which is composed of chl *a* and its epimer, chl *a*′.[2,3] A_0 reduces the secondary electron acceptor, A_1, which is a phylloquinone.[4] Sequential electron-transfer reactions then lead to the reduction of F_X, F_A, and F_B, which are iron−sulfur clusters. F_A and F_B are bound to the extrinsic PsaC subunit, while the other electron-transfer cofactors are bound to the intrinsic, membrane-associated PsaA and PsaB subunits.[2,3]

The structure of PSI from *Synechococcus elongatus* has been solved at 2.5 Å resolution by X-ray diffraction.[3] There are two phylloquinone acceptor molecules, which are located in pseudo-C_2 structurally symmetric positions. The two phylloquinone cofactors will be designated here as A_{1A} and A_{1B}, where the subscripts designate the subunit to which the phylloquinone molecule is bound. It has been proposed that both sets of phylloquinone cofactors are reduced in PSI electron-transfer reactions but with different time constants.[5−19] In *Chlamydomonas reinhardtii*, electron transfer has been deduced to be bidirectional with a 1:1 ratio of the kinetic phases.[6,8] In cyanobacteria, electron transfer is more unidirectional along the PsaA branch.[20−24] In particular, PSI from *Synechocystis PCC 6803* shows a fast phase (time constant 11 ns) and slow phase, which have been assigned to oxidation of A_{1B}^- and A_{1A}^-, respectively. The slow phase was observed to have a 340 ns time constant at 295 K and to slow upon cooling, with an activation energy of 110 meV.[25] The minor fast phase was observed to be temperature-independent.

The structure of phylloquinone is shown in Figure 1, along with its IUPAC numbering scheme. Figure 2 displays the binding pockets of A_{1A} (left) and A_{1B} (right) from the 2.5 Å PSI structure.[3] A predominant feature of both binding pockets is a tryptophan residue, which is within π-stacking distance of each A_1 acceptor. These two conserved tryptophans are located on the stromal side of A_{1A} and A_{1B}. The distances between the indole ring and the quinone are approximately 3 Å for A_{1A} and 3.5 Å for A_{1B}. Another striking feature of the A_1 protein environment is an asymmetric hydrogen bond from the amide NH groups of LeuA722 and LeuB706, respectively, to the C_4═O groups of each A_1 molecule.[3,26−28] The lack of a second hydrogen bond to C_1═O distinguishes the A_1 binding site, when compared to the Q_A binding site in bacterial reaction centers, in which two hydrogen bonds are formed to Q_A. A tryptophan−Q_A pi−pi interaction also occurs in the bacterial reaction center.[2,28−31]

* To whom correspondence should be addressed. E-mail: bridgette.barry@chemistry.gatech.edu.
‡ Georgia Institute of Technology.
† University of Oklahoma.

10.1021/jp0775146 CCC: $40.75 © 2008 American Chemical Society
Published on Web 02/29/2008

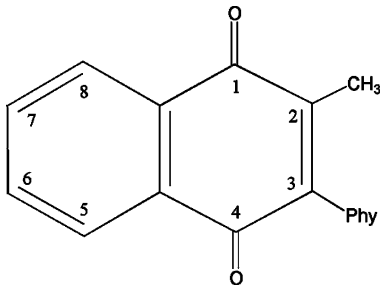

Figure 1. The structure of the secondary electron acceptor A_1 in photosystem I. Numbering is according to IUPAC nomenclature. Phy represents the phytol tail bonded to carbon 3.

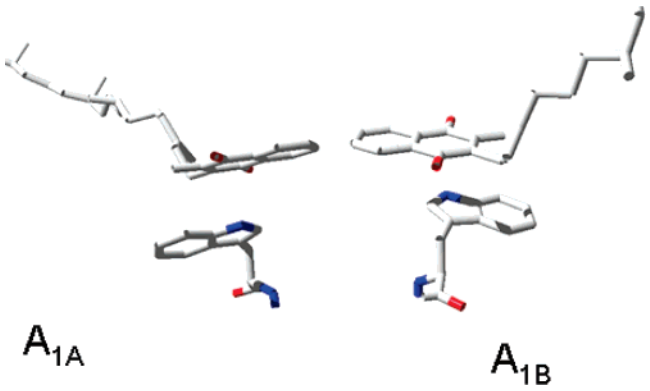

Figure 2. The binding site of A_{1A} (left) and A_{1B} (right) in photosystem I from the PSI crystal structure at 2.5 Å.[3] The tryptophan residues are within π-stacking distance (3−3.5 Å) of the quinone ring.

A_1 has the lowest known redox potential of any quinone found in nature. Measurements for the A_1 redox potential range from −750 to −810 mV.[32] Previous studies in which A_1 was exchanged for various quinone molecules, such as benzoquinone, have shown a −0.3 V change in the redox potential compared to the measured reduction potential in solution.[33] These results indicated that specific protein−cofactor interactions, such as the NH···CO asymmetric hydrogen bond[17,27,28,34] and possibly the pi−pi interaction, modulate the redox potential of quinones bound to the A_1 binding site.[35] Recent work has also implicated an electrostatic interaction with an aspartate as a modulator of the A_1 redox potential.[36]

To understand the structure of A_1/A_1^- and their interaction with the protein environment, we have used FT-IR spectroscopy. Vibrational spectroscopy supplies dynamic structural information concerning the electron-transfer cofactors. Previously, A_1/A_1^- spectra have been constructed, and multiple assignments have been suggested for the A_1 and A_1^- vibrational bands.[37−41] However, there are discrepancies in these assignments, and different spectroscopic methods have yielded contradictory results.

In this study, we have used isotopic labeling of phylloquinone in order to identify the vibrational modes of A_1 and A_1^-, under conditions in which A_1 is the terminal electron acceptor in PSI. When the iron−sulfur clusters, F_X, F_A, and F_B are removed, the $P_{700}^+A_1^-$ state can be photogenerated.[42−44] We have incorporated C^2H_3 into the methyl group of A_1 using a methionine-tolerant strain of the cyanobacterium, *Synechocystis sp. PCC 6803*. This approach has been used previously to assign bands to the plastoquinone acceptors, Q_A and Q_A^-, in cyanobacterial photosystem II.[45] In our current work, light-minus-dark FT-IR spectroscopy identifies C^2H_3-sensitive bands of A_1 and A_1^-. The data presented here support the interpretation that an asymmetric hydrogen bond, electrostatic interactions, and/or a pi−pi interaction shift the CO stretching and quinone ring stretching frequencies of A_1 and A_1^-, relative to model compounds.

Materials and Methods

Isotopic Labeling and PSI Purification. A methionine-tolerant strain of *Synechocystis PCC 6803* was grown on solid media, containing 90 μM methionine, BG-11, 5 mM TES−NaOH, pH 8.0, and 6 mM $Na_2S_2O_3$.[46,47] Liquid cultures (15 L) were supplemented either with 200 μM natural abundance C^1H_3 methionine or C^2H_3 methionine (98% enrichment, Cambridge Isotope Laboratories, Andover, MA).[45] Trimeric PSI was purified as described previously.[48] Purified trimeric PSI samples were dialyzed overnight in 5 mM HEPES−NaOH, pH 7.5, 0.04% dodecyl-β-D-maltoside (LM) and were concentrated using an Amicon (Bedford, MA) Ultra 100 000 MWCO centrifugal filter device to a final concentration of 4.6 mg chl/mL.

Apo-F_X Preparations. PSI (0.25 mg chl/mL) was incubated in a buffer containing 6.8 M urea, 50 mM Tris, 10 mM glycine−NaOH, pH 10, for 70 min, as previously described.[49] The PSI sample was then dialyzed overnight against 50 mM Tris−HCl, pH 8.3. The sample was incubated in 3 M urea, 5 mM K_3FeCN_6, 50 mM Tris−HCl, pH 8.3, for 2 h to remove the F_X cluster.[42] The sample was dialyzed overnight against 50 mM Tris−HCl, pH 8.3, and then again overnight against a buffer containing 50 mM Tris−HCl, pH 8.3, 5 mM 4,5-dihydroxy-1,3-benzene-disulfonic acid, which was supplied as the disodium salt. The sample was dialyzed a third night against 50 mM Tris, pH 8.3, 0.035% LM.[42,50,51] The sample was buffer exchanged with 5 mM HEPES−NaOH, pH 7.5, and concentrated using an Amicon Ultra 100 000 MWCO centrifugal filter device. The final chl concentration was 3 mg/mL.

Transient absorption spectroscopy, monitoring the decay of the P_{700}^+ signal at 820 nm, was performed to verify iron−sulfur cluster removal, as previously described.[42] The PSI concentration was 41−58 micrograms chl/mL, and the samples were in 50 mM Tris, pH 8.3, and 0.035% LM. Sodium ascorbate (5 mM) and 2,6-dichlorphenolindophenol (DCPIP, 5 μM) were added as exogenous electron donors. The 532 nm photolysis laser had an energy of 1.5−1.8 mJ/cm^2. SDS gel electrophoresis was also used to verify PsaC removal.[52,53]

Assessment of Isotope Enrichment through Mass Spectrometry. Previous quantitative work has shown that both the 13^4-methyl of chl[54] and the phylloquinone ring C_2 methyl group[55,56] are labeled from C^2H_3 methionine, which is a methyl group donor to both cofactors. Therefore, phylloquinone isotopic enrichment can be monitored indirectly by measuring the amount of chl isotopic labeling in cyanobacterial cultures grown on C^2H_3 methionine.[56] The control sample was isolated from cyanobacteria grown on natural abundance methionine. Chlorophyll was extracted from PSI with a solution of 80% acetone/20% methanol. The extracted pigments were vortexed, sonicated, centrifuged, and filtered as previously described.[57] Chlorophyll was concentrated and dried using a Thermo-Savant SpeedVac concentrator with VLP120 pump and RVT 400 refrigerated vapor trap (Thermo Electron Corporation, Waltham, MA). Chlorophyll samples were stored at −70 °C until use. Matrix-assisted laser desorption ionization mass spectrometry on a 4700 Proteomics analyzer (Applied Biosystems, Foster City, CA) was performed to determine the amount of C^2H_3 incorporation. Immediately before the measurement, chlorophyll was dissolved in a mixture of 80% methanol, 19% water, and 1% acetic acid;

this treatment removes the central Mg^{2+} ion of chlorophyll and generates pheophytin. The matrix used was alpha-cyano-4-hydroxy cinnamonic acid. The 871.5 *m*/*z* peak of pheophytin {M+H} was used for quantitation. Data were analyzed using IGOR (Wavemetrics, Lake Oswego, OR) software. The data were normalized to the M+H peak, and the isotope distribution was calculated. This approach gave 40 ± 1% labeling of the chlorophyll methyl group from C^2H_3 methionine and implied a similar amount of phylloquinone labeling.[55,56] Previous work has shown that there is no significant scrambling into other amino acids besides methionine, suggesting that there will be no detectable labeling of the peptide backbone.[45]

FT-IR Spectroscopy. FT-IR spectra were collected at −10 °C[58] or at room temperature (20 °C). Samples contained 3 mM potassium ferricyanide and 3 mM potassium ferrocyanide and were concentrated at room temperature under a steady flow of nitrogen gas. Concentration times were 20−30 min. Spectral conditions were as follows: resolution, 4 cm^{-1}; zero filling, 1; data acquisition time, 4.0 min. Difference spectra (light-minus-dark) were generated by taking the ratio of single-beam spectra collected before and during illumination and converting to absorbance. A_1^-/A_1 spectra were generated by subtraction of data from intact and apo-F_X PSI. The A_1^-/A_1 isotope-edited spectra were generated by subtracting difference FT-IR spectra of C^2H_3 apo-F_X PSI samples from difference FT-IR spectra, acquired from C^1H_3 apo-F_X PSI samples.[48,54,59] FT-IR spectra were obtained in the dark or under continuous illumination with red- and heat-filtered light, as previously described.[48,59] A 90 min dark relaxation time was used between successive illuminations. The final difference FT-IR spectra were an average (see figure legends) and were normalized for small differences in sample concentration and path length using the amplitude of the amide II band in the infrared absorption spectrum. The infrared absorption spectrum was created using a dark and a background scan, which was acquired with infrared windows, but no PSI sample. Previous studies have found that changes in hydration levels alter the details of PSI charge separation.[59] Therefore, water content in all of the FT-IR samples was held constant, as assessed by the ratio (1.1−1.3) of the 3300 cm^{-1} band to the amide I band at 1656 cm^{-1}.[48]

Density Functional Calculations. Density functional methods were used to predict the vibrational frequencies, IR intensities, and isotopic frequency shifts for the normal modes of models for phylloquinone and the phylloquinone anion radical. Figure 1 displays the structure of phylloquinone. For the model, the isoprenyl chain of phylloquinone was truncated to a single isoprenyl unit for ease in computation. The methyl group on the quinone ring was completely deuterated in order to estimate the maximum isotopic frequency shifts.

The B3LYP hybrid Hartree−Fock density functional (HF/DF) method[60] was used to calculate the vibrational frequencies for a model of phylloquinone and its radical anion. The B3LYP method was chosen because it is known to give harmonic vibrational frequencies within approximately 4% of experiment for approximately the same computer time investment as a Hartree−Fock calculation, in which estimated frequencies vary from experiment by more than 10%.[61] The three-parameter B3LYP method uses a weighted sum of Hartree−Fock, local DF, and gradient-corrected DF expressions for the exchange and correlation energies, where E_X^{Slater} is Slater's local spin density functional for exchange,[62] E_X^{Becke} is Becke's gradient correct exchange functional,[63] E_C^{VWN} is the local density correlation functional of Vosko, Wilk, and Nusair,[64] and E_C^{LYP} is the gradient-corrected correlation functional of Lee, Yang, and Parr.[65] Coefficients giving the relative weights of various approximations for the exchange and correlation energies in this method were optimized to reproduce thermochemical data for a variety of small molecules.[60] All calculations reported here were performed using the 6-31G(d) split-valence plus polarization basis set.[66,67] This basis set was chosen because it reproduces the properties of medium-sized organic molecules, including a variety of *p*-benzoquinones and their radical anions, and is small enough for rapid calculations.[68−73]

The quantum chemistry program Gaussian 03[74] was used for all calculations. Berny's optimization algorithm was used to perform full geometry optimizations in C_1 symmetry using internal coordinates.[75] Frequency calculations were performed for the optimized geometries. It has been customary to scale calculated vibrational frequencies, and we adopt the scaling factor of 0.9614 suggested by Scott and Radom.[61]

Vibrational mode assignments were performed by animating each mode using the program XMOL[76] and comparing the modes of one molecule to another using the program ViPA, an acronym for vibrational projection analysis.[71,72] The ViPA program[71,72] exploits the vector properties of vibrational normal modes to assess the similarity between modes of an object molecule and a structurally similar basis molecule. The program first aligns the two molecules and calculates each molecule's normal modes and vibrational frequencies. For each molecule, each of the normal vibrational modes is a column vector, which is orthonormal to all other normal modes of the same molecule. The vector projection operation is done by sequentially projecting each normal mode of the object molecule onto the modes of the basis molecule. The similarity of any mode of the object molecule to any mode of the basis molecule can then be expressed as a percentage by calculating the sum of the squares of the matrix elements and multiplying by 100. Vibrational projection analysis has been exploited to compare normal modes modified by isotopic substitution, oxidation/reduction, as well as covalent[72,77] and noncovalent[45,78] modifications.

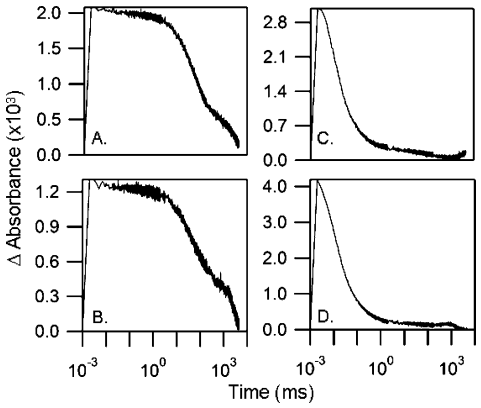

Figure 3. Decay of P_{700}^+, as assessed by 820 nm kinetic measurements, in (A) natural abundance C^1H_3-A_1 intact PSI, (B) labeled C^2H_3-A_1 intact PSI, (C) natural abundance C^1H_3-A_1 apo-F_X PSI, and (D) labeled C^2H_3 apo-F_X PSI. The reaction medium contained 50 mM Tris buffer (pH 8.3), 0.035% *n*-dodecyl-*β*-D-maltoside, 5 μM DCPIP, and 5 mM sodium ascorbate. See Materials and Methods for additional experimental details.

Results

Transient absorption experiments were performed to verify the removal of the iron−sulfur clusters in the apo-F_X samples. In the absence of F_X, F_A, and F_B, P_{700}^+ recombines with A_1^-, and an acceleration in the decay rate of P_{700}^+ is expected.[32,42,44,50,79−81] P_{700}^+ decay can be detected at 820 nm

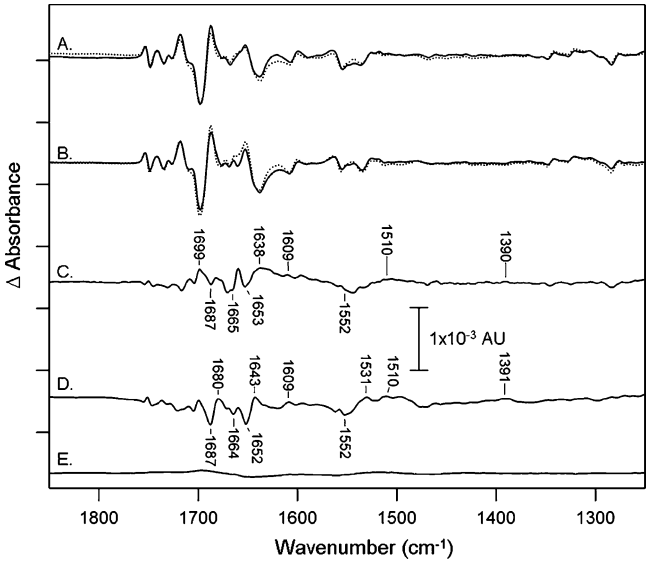

Figure 4. Light-induced FT-IR difference spectra of (A) natural abundance apo-F_X and (B) natural abundance intact PSI. Spectra were recorded either at room temperature (20 °C, solid lines) or at −10 °C (dotted lines). The data in B were divided by a factor of 3 to correct for a difference in the amount of stable charge separation. The room-temperature A_1^--minus-A_1 spectrum in C was constructed by subtracting B (solid line) from A (solid line). The −10 °C A_1^--minus-A_1 spectrum in D was constructed by subtracting B (dotted line) from A (dotted line). Spectrum E is room temperature, dark-minus-dark control, which was derived from the apo-F_X PSI data set. The solid lines in A, B, and E are the average of 21, 22, and 21 spectra, respectively. The dotted lines in A and B are the average of 45 and 27 spectra, respectively. See Materials and Methods for additional experimental details.

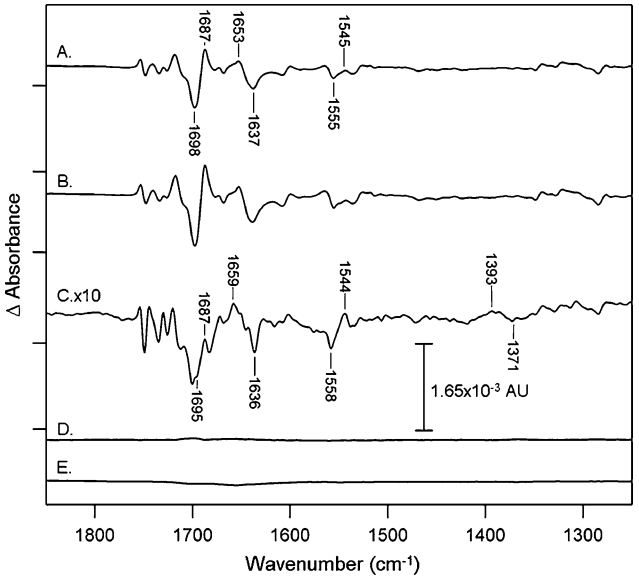

Figure 5. Light-induced FT-IR difference spectra of (A) natural abundance C^1H_3-A_1 apo-F_X PSI and (B) labeled C^2H_3-A_1 apo-F_X PSI. The isotope-edited spectrum shown in C is a C^1H_3-minus-C^2H_3 double difference spectrum created by subtraction of B from A and multiplying by a factor of 10. Spectrum D is a control double difference spectrum generated by taking one-half of the data in A, subtracting the other half of the data set, and dividing by $\sqrt{2}$. Spectrum (E) is a dark-minus-dark control. A, B, D, and E are the average of 45 spectra. See Materials and Methods for additional experimental details. The spectra were recorded at −10 °C.

(Figure 3) after a 532 nm flash. At the low 532 nm excitation energies employed here, previous work has shown that chl triplets do not make a significant contribution to 820 nm decay kinetics either in intact or apo-F_X PSI.[82] Therefore, the decay of 820 nm absorbance is attributed to P_{700}^+ recombination with PSI electron acceptors. The effects of changes in 532 nm excitation energy on intact and apo-F_X PSI have been previously described.[82]

Figure 3A and B shows P_{700}^+ decay kinetics in intact PSI samples, which contain F_X, F_A, and F_B. Figure 3A was obtained from cells cultured on C^1H_3 methionine; Figure 3B was obtained from cells cultured on C^2H_3 methionine. These intact samples show the expected P_{700}^+ F_A^-/F_B^- recombination kinetics[42,50] with lifetimes of 15−18 and 84−95 ms. A third slower phase (lifetime 4−6 s) is assigned to the reduction of P_{700}^+ by the exogenous electron donor, DCPIP. Figure 3C and D exhibits the P_{700}^+ decay kinetics, which were measured in apo-F_X PSI. Figure 3C was obtained from cells cultured on C^1H_3 methionine, and Figure 3D was obtained from cells cultured on C^2H_3 methionine. In Figure 3C and D, the lifetime of P_{700}^+ has decreased dramatically, as predicted for samples with A_1 as the terminal electron acceptor. The slow phases of 15−18 and 84−96 ms have been replaced by faster biphasic kinetics with lifetimes of 11−13 and 69−115 μs.[83] These results demonstrate that F_A, F_B, and F_X have been removed in the apo-F_X preparation.

In Figure 4, we present difference (light-minus-dark) FT-IR spectra acquired either from apo-F_X (Figure 4A) or intact PSI (Figure 4B) at room temperature (solid lines) or at −10 °C (dotted lines). The data in Figure 4A correspond to $P_{700}^+A_1^-$-minus-$P_{700}A_1$ spectra, and the data in Figure 4B correspond to $P_{700}^+F_B^-$-minus-$P_{700}F_B$ spectra. The spectrum in Figure 4A is in good agreement with previously published time-resolved spectra of P_{700}^+/A_1^-, confirming the accumulation of the A_1^- species[38,39] and the generation of P_{700}^+ and not the P_{700} triplet, $^3P_{700}$.[38,84]

In Figure 4C (room temperature) and Figure 4D (−10 °C), construction of the double difference spectrum, A_1^--minus-A_1, was performed by subtraction of data in Figure 4B from that in Figure 4A. In construction of these double difference spectra, data in Figure 4B were divided by a factor of 3 to account for an overall difference in spectral amplitude in the two PSI preparations. The increased spectral amplitude in Figure 4B, compared to that in Figure 4A, may be attributable to an increased efficiency of charge separation in intact PSI compared to apo-F_X PSI under the low-intensity, continuous, red-filtered illumination used for the FT-IR measurements.

In the resulting double difference spectra (Figure 4C and Figure 4D), unique vibrational bands of A_1 appear as negative signals; unique vibrational contributions from A_1^- are positive bands. The reduction spectrum of F_B is not expected to contribute significantly in this spectral region.[84] Figure 4 demonstrates that the A_1^--minus-A_1 spectra acquired at room temperature and −10 °C are similar (Figure 4C and D), except for an increased amplitude at ∼1620 cm^{-1} in the room-temperature data, which may be due to an increased contribution from water at the higher temperature (Figure 4C). Previously, the difference FT-IR A_1^--minus-A_1 spectrum has been reported in apo-F_X PSI preparations at room temperature. Comparison of our data with this previously reported work is difficult due to the use of ^2H_2O buffers in ref 37. However, the spectra in Figure 4C and D do show similarities to the transient spectrum, attributed to A_1^--minus-A_1, in intact cyanobacterial PSI. The transient spectrum was acquired by microsecond, time-resolved, step-scan FT-IR techniques in ^1H_2O buffers at 77 K.[38]

In Figure 5, we present difference (light-minus-dark) FT-IR spectra obtained from apo-F_X PSI samples and attributable to

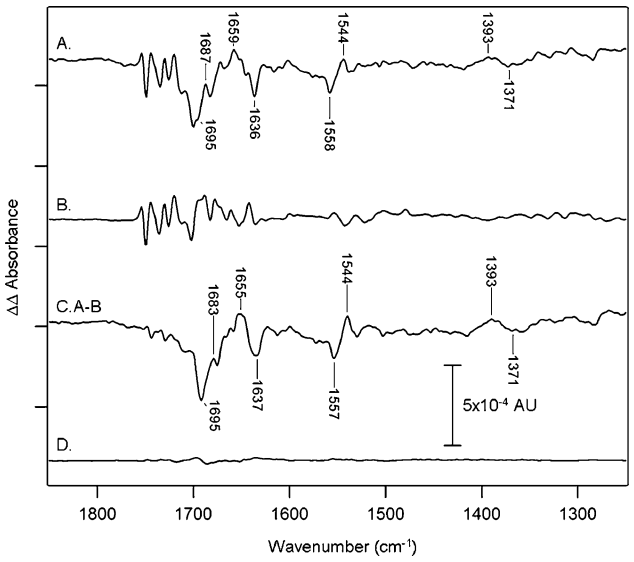

Figure 6. Isotope-edited FT-IR spectra of PSI. (A) shows the C^1H_3-minus-C^2H_3 double difference spectrum, acquired from apo-F_X PSI (average of 45 spectra), (B) shows the C^1H_3-minus-C^2H_3 double difference spectrum, acquired from intact PSI (average of 27 spectra), and (C) shows a subtraction of A minus B, revealing isotopic shifts in the A_1^- (positive) and A_1 (negative) bands. The spectra in A and B were normalized to give the same intensity in the P_{700}^+ ester vibrational bands between 1752 and 1748 cm^{-1}. Spectrum D is a control double difference spectrum generated by taking one-half of the data in A, subtracting the other half of the data set, and dividing by $\sqrt{2}$. See Materials and Methods for additional experimental details. The spectra were recorded at −10 °C.

$P_{700}^+A_1^-$-minus-$P_{700}A_1$. Figure 5A shows the difference spectrum acquired from the natural abundance C^1H_3 phylloquinone control, which was isolated from cells cultured on C^1H_3 methionine. Figure 5B shows the spectrum acquired from C^2H_3-phylloquinone-labeled samples. The isotope-edited C^1H_3-minus-C^2H_3 double difference spectrum (Figure 5C) was constructed by subtraction of Figure 5B from 5A and was multiplied by a factor of 10 for presentation. C^2H_3-induced shifts are observed as derivative-shaped spectral features. To appear in the isotope-edited spectrum, the frequencies must be perturbed by charge separation (for example, by the reduction of A_1) and by isotope incorporation. Figure 5D shows a control subtraction that was generated by subtracting one-half of the C^1H_3−PSI data set from the other half of the data set. The spectrum will not contain any vibrational bands and allows an estimate of the noise in the averaged data. Comparison of Figure 5C and D demonstrates that the vibrational frequencies observed in Figure 5C are significant. Figure 5E is the dark-minus-dark spectrum, showing that the observed spectra in Figure 5A and B are dependent on illumination of the sample.

Both the 13^4-methyl of chl and the phylloquinone ring C_2 methyl group (Figure 1) are labeled from methionine.[54,55] Chl methyl labeling has been shown to shift the ester and keto vibrational bands of P_{700}^+-minus-P_{700}.[54] The ester vibrational bands of P_{700}^+-minus-P_{700} have been previously assigned to spectral features observed between 1760 and 1700 cm^{-1},[54] and in Figure 5C, the expected spectral shifts due to the P_{700}/P_{700}^+ ester bands are observed. Therefore, the isotope-edited spectrum in Figure 5C exhibits contributions from isotope labeling of P_{700}, as well as from labeling of A_1.

To identify isotope shifts due to A_1/A_1^- alone, the isotope-edited spectrum derived from intact PSI (Figure 6B) was subtracted from the isotope-edited spectrum derived from apo-F_X PSI (Figure 6A), after normalization for the chl ester bands. This normalization accounts for the lower amplitude of the difference spectrum, acquired from the apo-F_X preparation. This lower amplitude may be due to a smaller amount of charge separation in the apo-F_X preparation, as described above. The resulting isotope-edited spectrum (Figure 6C) will reflect isotope-induced shifts in vibrational bands of A_1 and A_1^-. Unique vibrational bands of A_1 appear as negative signals, with the corresponding isotope-shifted components appearing as positive bands. Unique vibrational contributions from A_1^- are positive bands; the corresponding isotope-shifted components are negative bands. Figure 6D shows a negative control, in which no vibrational bands are expected.

To assign spectral features in Figure 6C to normal modes of the phylloquinone singlet and anion radical, DFT calculations were used to predict the frequencies, intensities, and C^2H_3 isotope shifts. The predicted frequencies and intensities are in reasonable agreement with those reported previously.[39] Of particular interest are the carbonyl and quinone ring stretching vibrations (Table 1), which have frequencies and intensities that may respond to environmental perturbations, such as hydrogen bonding, electrostatic interactions, and pi−pi stacking. Table 1 shows that only the CO stretching and CC quinoid ring stretching vibrations are predicted to have vibrational frequencies that are sensitive to phylloquinone reduction. Aromatic ring modes are expected to cancel approximately in the difference spectrum due to the lack of a reduction-induced frequency shift and are not considered further. The CO antisymmetric stretching vibration is predicted to be the most intense band both in the singlet and the anion spectrum (Table 1). Although, in principle, two CO bands are expected, the symmetric CO vibrational mode is predicted to be significantly less intense compared to the antisymmetric mode, and the frequencies are predicted to be similar (Table 1). Therefore, the two CO bands may overlap in the experimental spectrum. Upon phylloquinone reduction, the CO band is predicted to downshift by 174 cm^{-1}. The most intense quinoid CC stretching vibration is predicted to downshift by 100 cm^{-1} and to change from a "symmetric" stretch (predominantly C_2C_3 stretching) to an "antisymmetric" stretch (mainly C_9C_{10} stretching). The predicted isotope shifts in Table 1 are accurate only to approximately 5 cm^{-1}, and therefore, the expected isotope-induced downshifts for these bands are similar and less than 8 cm^{-1}. The CO and quinoid normal modes are predicted to have similar intensities both in the singlet and in the anion spectrum and thus should be observable in the isotope-edited spectrum.

On the basis of comparison to these DFT calculations, bands in Figure 6C are assigned to A_1^- and A_1 in Table 1. For comparison, previous experimental assignments of phylloquinone singlet and anion radical bands are summarized in Table 2.[37,38,85−87] In our isotope-based assignments, a negative−positive−negative complex spectral feature is observed with frequencies of 1695 (neg.), 1655 (pos.), and 1637 (neg.) cm^{-1} (Figure 6C). The data were simulated by the generation of Gaussian curves (data not shown). These simulations were dominated by two bands centered at 1688 (neg.) and 1685 (pos.) cm^{-1}, which we assign to the singlet CO stretching vibration and its induced isotope shift. The complexity of the observed spectral line shape may be due to overlapping contributions from the CO antisymmetric and symmetric stretching vibrations in each of two A_1 molecules (Table 1). Our scaled DFT calculations predict a frequency of 1672 cm^{-1} for the CO antisymmetric vibrational mode, supporting this assignment.

The singlet quinoid CC stretching mode is predicted (Table 1) with reasonable intensity at 1610 (scaled) cm^{-1}. Therefore,

TABLE 1: Assignments of A_1 and A_1^- Vibrational Bands, Based on Isotopic Labeling of the Phylloquinone Acceptor and DFT Calculations

singlet	frequency[a] C^1H_3	frequency C^2H_3	Δ C^2H_3	predicted[b] frequency C^1H_3	predicted[b,c] Δ C^2H_3	predicted[b] intensity C^1H_3
CO antisymmetric stretching	1688	1685	3	1672	0	270
CO symmetric stretching	NA[d]	NA	−	1666	0	26
aromatic ring stretching	NA	NA	−	1584	1	52
quinoid "symmetric"[d] stretching[e]	1557	1544	13	1610	3	42
quinoid "antisymmetric"[d] stretching[e]	NA	NA	−	1571	1	2
anion radical	**frequency C^1H_3**	**frequency C^2H_3**	**Δ C^2H_3**	**predicted[b] frequency C^1H_3**	**predicted[b] Δ C^2H_3**	**predicted[b] intensity C^1H_3**
quinoid antisymmetric[d] stretching	NA	NA	−	1510	1	35
quinoid symmetric[d] stretching	NA	NA	−	1576	1	3
aromatic ring stretching	NA	NA	−	1585	0	3
CO antisymmetric stretching	1393	1371	22	1498	1	310
CO symmetric stretching	NA	NA	−	1483	8	17

[a] Frequencies reported in wavenumber (cm^{-1}). [b] Predicted frequencies (scaled by 0.9614), isotope shifts (Δ C^2H_3), and intensities from DFT calculations. [c] Predicted shifts accurate to ± 5 cm^{-1}. [d] NA, not assigned. [e] Although singlet quinoid stretching modes are labeled "symmetric" and "antisymmetric", the modes are mixed and highly localized. Thus, the "symmetric" mode contains predominantly C_2C_3 stretching, whereas the "antisymmetric" stretch contains predominantly C_9C_{10} stretching. [d] The pseudosymmetry plane contains the CO bonds.

the negative spectral feature at 1557 cm^{-1} in Figure 6C is assigned to the A_1 quinoid ring stretching vibration. The corresponding isotope-shifted component is shifted in the predicted direction, but the magnitude of the shift is larger than predicted (Table 1). This observation suggests significant motion of the methyl group in these singlet CO and quinoid normal modes. This is supported by the fact that the calculated mode also contains some methyl group motion.

As discussed above, the CO stretching vibration is predicted to be the most intense A_1^- band (Table 1). In Figure 6C, the only positive band, which is assignable to the A_1^- CO, is at 1393 cm^{-1}. Therefore, the broad spectral features (Figure 6C) at positive 1393 cm^{-1} and negative 1371 cm^{-1} are assigned to the CO vibration of the anion and its isotope-shifted component (Table 1). Broadening of these bands may be due to overlapping contributions from two A_1^- molecules and from the antisymmetric and symmetric CO bands. The scaled CO antisymmetric stretching frequency (Table 1) predicts a frequency of 1498 cm^{-1} for this mode. We speculate that the lower than expected intensity and frequency for the CO band (Table 1) may be due to the asymmetric hydrogen bond, an electrostatic interaction, or to the pi−pi interaction with the quinone binding site tryptophan (see Discussion below). In Figure 6C, candidates for the quinoid CC stretching vibrations are not observed in the expected 1500−1400 cm^{-1} spectral region, perhaps because the isotope shifts are small and the bands have low intrinsic intensity (Table 1).

Discussion

In this work, we have incorporated C^2H_3 into the C_2 methyl group of the A_1 electron acceptor, and we have used this approach to assign vibrational bands to A_1^- and A_1. This experiment was performed in apo-F_X PSI preparations, in which A_1 is the terminal electron acceptor.[42,51] Previous studies have shown that inactivation of the rubA gene resulted in PSI complexes lacking the stromal subunits, PsaC, PsaD, and PsaE. Furthermore, this mutant was unable to assemble F_X.[44] This work led to the conclusion that removal of the iron−sulfur clusters does not appreciably alter the orientation of A_1^- or the distance between A_1^- and P_{700}^+. However, that study did find that the motion of A_1 in the mutants may be greater due to the absence of F_X and the stromal subunits.[44] Previous work studying chemically extracted $P_{700}-A_1$ core proteins has concluded that there is a change in the A_1 hydrogen-bonding environment.[42−44,51] However, our approach of using apo-F_X samples has the advantage of simplifying the spectrum, increasing the amplitude of A_1^- spectral contributions, and avoiding complex spectral deconvolution techniques, which are required to study A_1^- in intact PSI, where the anion radical has a short lifetime.[80]

The PSI crystal structure (Figure 2) reveals that the C_1O groups of the A_1 acceptors do not participate in hydrogen bonding. However, the C_4O groups accept a hydrogen bond from the backbone NH group of LeuA722 for A_{1A} or LeuB706 for A_{1B}.[2,3,27,28,88] EPR studies have shown asymmetric hydrogen bonding to A_1^- and an asymmetric distribution of spin density.[26−28,44,89] This result suggests that the hydrogen bond to C_4O is sustained upon reduction of A_1. Evidence for a pi−pi stacking interaction with a nearby tryptophan comes from analysis of the PSI structure and from EPR and mutational studies.[2,3,8,9,90]

Our assignments, which are presented in Table 1, are based on DFT calculations as well as isotope labeling of the phylloquinone molecule. An analysis of these results and comparison to previous work is presented below.

Comparison to Previous A_1/A_1^- Assignments in apo-F_X PSI. Our results, based on phylloquinone labeling, are congruent with previous interpretations of the apo-F_X A_1/A_1^- spectrum at room temperature (Table 2).[37] In those experiments, a 1680 cm^{-1} band was assigned to the C_1O stretching of A_1; the hydrogen-

TABLE 2: Previous Assignments of Phylloquinone Singlet and Anion Radical IR Bands

in vitro phylloquinone vibrational assignments			
description of normal mode	solvent and sample type	singlet (cm^{-1})	anion radical (cm^{-1})
carbonyl stretching	CH_2Cl_2[85]	1658, 1616	1488
quinoid stretching	CH_2Cl_2[85]	1596	NA[a]
aromatic ring stretching	CH_2Cl_2[85]	1596	NA
carbonyl stretching	film[86]	1661	NA
quinone stretching	film[86]	1618	NA
aromatic stretching	film[86]	1597	NA
bacterial reaction center vibrational assignments			
description of normal mode	bacterial reaction center sample	singlet (cm^{-1})	anion radical (cm^{-1})
carbonyl stretching	*Rb. viridis*[87]	1653, 1637	1438
quinoid stretching	*Rb. viridis*[87]	1609−1608	NA
aromatic ring stretching	*Rb. viridis*[87]	1590	NA
carbonyl stretching	*Rb. sphaeroides*[86]	1651, 1640	1444
quinoid stretching	*Rb. sphaeroides*[86]	1608	1478, 1394−1388
aromatic ring stretching	*Rb. sphaeroides*[86]	1588	1478, 1394−1388
photosystem I vibrational assignments			
description of normal mode	photosystem I sample	singlet (cm^{-1})	anion radical (cm^{-1})
carbonyl stretching	intact[38]	1655, 1607	1495
quinoid stretching	intact[38]	1651, 1634	1414
aromatic ring stretching	intact[38]	1651, 1634	1414
carbonyl stretching	apo−F_X[37]	1680, 1650, 1643	1455, 1445
quinoid stretching	apo−F_X[37]	NA	1396, 1381
aromatic ring stretching	apo−F_X[37]	NA	1396, 1381

[a] NA, not assigned.

bonded C_4O groups were assigned at 1643 and 1650 cm^{-1}. The previously assigned 1680 cm^{-1} band may correspond to our 1688 cm^{-1} band. The previous 1643 cm^{-1} assignment may correspond to the negative 1637 cm^{-1} band, which we observe in our data. The A_1^- CO stretching frequencies were assigned at 1455 and 1445 cm^{-1} in that previous work (Table 2). A band at 1396 cm^{-1} was observed but assigned to a CC stretching vibration of the anion radical. Because our DFT calculations indicate that the most intense A_1^- band will be the CO antisymmetric stretching vibration, we favor the assignment of our 1393 cm^{-1} band to a carbonyl stretching vibration. Other, previously reported bands in the 1500−1400 cm^{-1} region (Table 2) are predicted by our calculations to be less isotope-sensitive and are not observed here with significant intensity.

Comparison to Previous A_1^-/A_1 Assignments in Intact PSI. Recently, A_1^-/A_1 spectra were generated using time-resolved FT-IR measurements at 77 K in intact PSI. Overall, the spectra exhibit similarities to the A_1^-/A_1 data reported here. However, in this previous time-resolved work, bands at 1655 and 1607 cm^{-1} were identified as the A_1 CO stretching vibrations (Table 2), consistent with two distinct carbonyl stretching vibrations for A_1. Quinoid CC stretching and benzene aromatic stretching vibrations were assigned at 1651 and 1634 cm^{-1}. Upon anion formation, the CO stretching and CC stretching vibrational bands were assigned at 1495 and 1414 cm^{-1}, respectively.[38] These assignments are in contrast to ours (Tables 1), as well as to previous assignments derived from FT-IR studies of apo-F_X PS1 (Table 2 and ref 37). These differences could arise from the deconvolution of the complex, time-resolved FT-IR spectrum, which was interpreted to contain chl A_0 keto vibrational bands in the 1680 cm^{-1} region.[38] It is also possible that removal of the polypeptides PsaC, PsaD, and PsaE and F_X causes subtle changes in the binding pocket of A_1, which are reflected in the vibrational frequencies of A_1 and A_1^- in the apo-F_X preparation.

Comparison to Previous Studies of Model Phylloquinone and Phylloquinone Anion Radicals In Vitro. Previous electrochemical FT-IR studies of phylloquinone in vitro assigned two singlet CO stretching vibrations at 1658 and 1616 cm^{-1} (Table 2) and an aromatic ring stretching vibration at 1596 cm^{-1}. Upon quinone reduction, the anion CO stretching band was observed at 1488 cm^{-1}, and the quinoid stretching was not assigned.[85] However, a second FT-IR study of phylloquinone (Table 2) have observed only one singlet CO stretching band at 1661 cm^{-1}, in agreement with our predictions (Table 1). In this second study, the quinoid stretching was assigned at 1618 cm^{-1}, and the aromatic ring stretching band was assigned at 1597 cm^{-1}.[86]

We assign the A_1 CO vibration at 1688 cm^{-1}, the A_1 quinoid stretching vibration at 1557 cm^{-1}, and the A_1^- CO vibration at 1393 cm^{-1} (Table 1). Compared to previous model compound work (Table 2), these data suggest significant environmental perturbations of A_1 and A_1^- in PSI. This environmental perturbation upshifts the singlet CO stretching vibration (by ∼30 cm^{-1}), downshifts the singlet quinoid ring vibration (by ∼60 cm^{-1}), and downshifts the radical CO vibration (by ∼95 cm^{-1}).

Comparison to Previous Studies of Phylloquinone in the Bacterial Reaction Center. In the bacterial reaction center, phylloquinone can be substituted and can function as the primary quinone acceptor, Q_A. In contrast to the PSI A_1 acceptor, in the bacterial reaction center, two hydrogen bonds are formed, one to each Q_A carbonyl oxygen. In *R. viridis*, it has been reported that the Q_A carbonyl oxygens are hydrogen bonded to the peptide NH of AlaM258 and to a non-heme iron histidine ligand.[29] In *R. sphaeroides*, it has been reported that the quinone carbonyl oxygens are hydrogen bonded to the peptide NH of AlaM258 and to ThrM222.[31] The indole group of a tryptophan is nearly parallel to the Q_A ring at a distance of 3.1 Å.[29,31]

When phylloquinone was substituted into the Q_A binding site in the bacterial reaction center,[86,87] two CO bands were observed, with frequencies at ∼1650 and 1640 cm^{-1} (Table 2). These bands were attributed to the antisymmetric CO vibration of the two different carbonyl groups, which have different frequencies due to differential hydrogen bonding.[86,87] The anion CO band

was assigned either at 1438 or 1444 cm^{-1}, ~50 cm^{-1} lower in frequency compared to the in vitro phylloquinone studies and ~50 cm^{-1} higher in frequency compared to our assignments for A_1^- (Table 1 and 2).

Rationalization of Environmental Perturbations to the A_1 and A_1^- Vibrational Spectra. We suggest that observed perturbations, when PSI is compared to model compounds or to phylloquinone-substituted bacterial reaction centers, are due to a combination of the asymmetric hydrogen-bonding pattern, electrostatic interactions, and the pi−pi stacking interaction with a tryptophan (Figure 2). We propose that these protein−quinone interactions have differential effects on the anion and singlet CO vibrational bands.

From the crystal structure, the secondary electron acceptor A_1 is known to be in pi−pi stacking distance with a tryptophan residue. The distance between the aromatic ring system of the Trp residues, TrpA697 and TrpB677, and the quinone A_{1A} and A_{1B} range between 3 and 3.5 Å, respectively.[2] Previous ESEEM studies have suggested a quinone−tryptophan interaction because it was shown that the unpaired electron on A_1^- is coupled to the nitrogen of tryptophan.[90,91] An increase in the g_X tensor component of A_1^-, compared to that of phylloquinone in solution, has been interpreted to imply that A_1 exists in a negative electrostatic environment.[36,92] Quantum chemical calculations have suggested that a fixed pi-stacked arrangement, as observed in the PSI structure, may lower the redox potential of the A_1 electron acceptor.[93] A charged aspartate may also modify the quinone redox potential.[36]

It should be noted that in model studies, symmetric hydrogen bonding in protic solvents had little effect on phylloquinone ring or CO frequencies.[85] In phylloquinone-substituted bacterial reaction centers, two hydrogen bonds to phylloquinone produced a splitting of only 10 cm^{-1} in the CO vibrational bands.[86,87] In addition, DFT calculations have predicted only small splittings and shifts of the CO vibrational bands (6−14 cm^{-1}) when an asymmetric hydrogen bond to phylloquinone and the phylloquinone anion radical is included in a simple model system.[40] However, prediction of the spectral changes due to the introduction of an unusual, asymmetric hydrogen bond awaits more detailed theoretical approaches based on the PSI structure, which must also include the effect of electrostatic or Stark interactions on the vibrational spectrum.[94]

Pi−pi interactions have complex effects on vibrational frequencies, perhaps due to difficulties in separating the effects of hydrogen bonding, geometry, dispersive, and electrostatic interactions in many biologically relevant systems.[59,95−100] Therefore, the expected effects of pi−pi interactions on quinone and tryptophan vibrational frequencies and amplitudes must also be addressed in future studies. Currently, DNA base stacking provides one possible model system for assessing the effect of pi−pi interactions. IR studies of polyuracil/polyadenine have shown that shifts of IR bands occur with helix formation. The uracil CO stretching frequency increased by 19 cm^{-1}, and the uracil ring stretching vibration decreased in frequency.[101] The transition from nonordered to ordered structures was observed to shift the carbonyl vibration toward higher frequency.[102] Studies of 1,3-dimethyluracil, cytidine, caffeine, inosine, and 2′-deoxyadenosine found that stacking of these molecules also had an effect on the IR spectra. The carbonyl stretching band increased in frequency, and a decrease in the intensity of the skeletal ring stretching vibrational bands were observed.[103] These experimental results concerning the effect of pi stacking on nucleobases are congruent with our A_1/A_1^- assignments.

Abbreviations

A_1, phylloquinone acceptor in photosystem I; chl, chlorophyll; DFT, density functional theory; EPR, electron paramagnetic resonance; FT-IR, Fourier transform infrared; PSI, Photosystem I; Q, quinone.

Acknowledgment. Supported by NIH GM43273 (B.A.B.) and the Oklahoma Supercomputing Center for Education and Research (OSCER). The authors thank Dr. J. Golbeck and Dr. R. Agalarov for performing the transient absorption measurements.

References and Notes

(1) Holzwarth, A. R.; Muller, M. G.; Niklas, J.; Lubitz, W. *Biophys. J.* **2006**, *90*, 552−565.
(2) Fromme, P.; Jordan, P.; Krauss, N. *Biochim. Biophys. Acta* **2001**, *1507*, 5−31.
(3) Jordan, P.; Fromme, P.; Witt, H. T.; Klukas, O.; Saenger, W.; Krauss, N. *Nature* **2001**, *411*, 909−917.
(4) Rustandi, R. R.; Snyder, S. W.; Feezel, L. L.; Michalski, T. J.; Norris, J. R.; Thurnauer, M. C.; Biggins, J. *Biochemistry* **1990**, *29*, 8030−8032.
(5) Rigby, S. E. J.; Evens, M. C. W.; Heathcote, P. *Biochemistry* **1996**, *35*, 6651−6656.
(6) Joliot, P.; Joliot, A. *Biochemistry* **1999**, *38*, 11130−11136.
(7) Boudreaux, B.; MacMillan, F.; Teutloff, C.; Agalarov, R.; Gu, F.; Grimaldi, S.; Bittl, R.; Brettel, K.; Redding, K. *J. Biol. Chem.* **2001**, *276*, 37299−37306.
(8) Guergova-Kuras, M.; Boudreaux, B.; Joliot, A.; Joliot, P.; Redding, K. *Proc. Natl. Acad. Sci. U.S.A.* **2001**, *98*, 4437−4442.
(9) Purton, S.; Stevens, D. R.; Muhiuddin, I. P.; Evans, M. C. W.; Carter, S.; Rigby, S. E. J.; Heathcote, P. *Biochemistry* **2001**, *40*, 2167−2175.
(10) Rigby, S. E. J.; Muhiuddin, I. P.; Evans, M. C. W.; Purton, S.; Heathcote, P. *Biochim. Biophys. Acta* **2002**, *1556*, 13−20.
(11) Ramesh, V. M.; Gibasiewicz, K.; Lin, S.; Bingham, S. E.; Webber, A. N. *Biochemistry* **2004**, *43*, 1369−1375.
(12) Bautista, J. A.; Rappaport, F.; Guergova-Kuras, M.; Cohen, R. O.; Golbeck, J. H.; Wang, J. Y.; Beal, D.; Diner, B. A. *J. Biol. Chem.* **2005**, *280*, 20030−20041.
(13) Poluektov, O. G.; Paschenko, S. V.; Utschig, L. M.; Lakshmi, K. V.; Thurnauer, M. C. *J. Am. Chem. Soc.* **2005**, *127*, 11910−11911.
(14) Santabarbara, S.; Heathcote, P.; Evans, M. C. W. *Biochim. Biophys. Acta* **2005**, *1708*, 283−310.
(15) Santabarbara, S.; Kuprov, I.; Fairclough, W. V.; Purton, S.; Hore, P. J.; Heathcote, P.; Evans, M. C. W. *Biochemistry* **2005**, *44*, 2119−2128.
(16) Ali, K.; Santabarbara, S.; Heathcote, P.; Evans, M. C. W.; Purton, S. *Biochim. Biophys. Acta* **2006** *1757*, 1623−1633.
(17) Li, Y.; van der Est, A.; Lucas, M. G.; Ramesh, V. M.; Gu, F.; Petrenko, A.; Lin, S.; Webber, A. N.; Rappaport, F.; Redding, K. *Proc. Natl. Acad. Sci. U.S.A.* **2006**, *103*, 2144−2149.
(18) Santabarbara, S.; Kuprov, I.; Hore, P. J.; Casal, A.; Heathcote, P.; Evans, M. C. W. *Biochemistry* **2006**, *45*, 7389−7403.
(19) Ramesh, V. M.; Gibasiewicz, K.; Lin, S.; Bingham, S. E.; Webber, A. N. *Biochim. Biophys. Acta* **2007**, *1767*, 151−160.
(20) Klughammer, C.; Klughammer, B.; Pace, R. *Biochemistry* **1999**, *38*, 3726−3732.
(21) Xu, W.; Chitnis, P. R.; Valieva, A.; van der Est, A.; Brettel, K.; Guergova-Kuras, M.; Pushkar, Y. N.; Zech, S. G.; Stehlik, D.; Shen, G.; Zybailov, B.; Golbeck, J. H. *J. Biol. Chem.* **2003**, *278*, 27876−27887.
(22) Xu, W.; Chitnis, P.; Valieva, A.; van der Est, A.; Pushkar, Y. N.; Krzystyniak, M.; Teutloff, C.; Zech, S. G.; Bittl, R.; Stehlik, D.; Zybailov, B.; Shen, G.; Golbeck, J. H. *J. Biol. Chem.* **2003**, *278*, 27864−27875.
(23) Cohen, R. O.; Shen, G.; Golbeck, J. H.; Xu, W.; Chitnis, P. R.; Valieva, A. I.; van der Est, A.; Pushkar, Y.; Stehlik, D. *Biochemistry* **2004**, *43*, 4741−4754.
(24) Dashdorj, N.; Xu, W.; Cohen, R. O.; Golbeck, J. H.; Savikhin, S. *Biophys. J.* **2005**, *88*, 1238−1249.
(25) Agalarov, R.; Klaus, B. *Biochim. Biophys. Acta* **2003**, *1604*, 7−12.
(26) Teutloff, C.; Bittl, R.; Lubitz, W. *Appl. Magn. Res.* **2004**, *26*, 5−21.
(27) Pushkar, Y. N.; Golbeck, J. H.; Stehlik, D.; Zimmermann, H. *J. Phys. Chem. B* **2004**, *108*, 9439−9448.
(28) Pushkar, Y.; Stehlik, D.; van Gastel, M.; Lubitz, W. *J. Mol. Struct.* **2004**, *700*, 233−241.
(29) Deisenhofer, J.; Michel, H. *Science* **1989**, *245*, 1463−1473.
(30) Kamlowski, A.; Altenberg-Greulich, B.; van der Est, A.; Zeck, S. G.; Bittl, R.; Fromme, P.; Lubitz, W.; Stehlik, D. *J. Phys. Chem. B* **1998**, *102*, 8278−8287.
(31) Allen, J. P.; Feher, G.; Yeates, T. O.; Komiya, H.; Rees, D. C. *Proc. Natl. Acad. Sci. U.S.A.* **1988**, *85*, 8487−8491.

(32) Brettel, K. *Biochim. Biophys. Acta* **1997**, *1318*, 322−373.
(33) Itoh, S.; Iwaki, M.; Ikegami, I. *Biochim. Biophys. Acta* **2001**, *1507*, 115−138.
(34) Feldman, K. S.; Hester, D. K., II; Golbeck, J. H. *Bioorg. Med. Chem. Lett.* **2007**, *17*, 4891−4894.
(35) van der Est, A. *Biochim. Biophys. Acta* **2001**, *1507*, 212−225.
(36) Karyagina, I.; Pushkar, Y.; Stehlik, D.; van der Est, A.; Ishikita, H.; Knapp, E. W.; Jagannathan, B.; Agalarov, R.; Golbeck, J. *Biochemistry* **2007**, *46*, 10804−10816.
(37) Hastings, G.; Sivakumar, V. *Biochemistry* **2001**, *40*, 3681−3689.
(38) Sivakumar, V.; Wang, R.; Hastings, G. *Biochemistry* **2005**, *44*, 1880−1893.
(39) Bandaranayake, K. M. P.; Sivakumar, V.; Wang, R.; Hastings, G. *Vib. Spectrosc.* **2006**, *42*, 78−87.
(40) Bandaranayake, K. M. P.; Wang, R.; Hastings, G. *Biochemistry* **2006**, *45*, 4121−4127.
(41) Bandaranayake, K. M. P.; Wang, R.; Johnson, T. W.; Hastings, G. *Biochemistry* **2006**, *45*, 12733−12740.
(42) Warren, P. V.; Parrett, K. G.; Warden, J. T.; Golbeck, J. H. *Biochemistry* **1990**, *29*, 6545−6550.
(43) van der Est, A.; Bock, C.; Golbeck, J.; Brettel, K.; Setif, P.; Stehlik, D. *Biochemistry* **1994**, *33*, 11789−11797.
(44) Shen, G.; Antonkine, M. L.; van der Est, A.; Vassiliev, I. R.; Brettel, K.; Bittl, R.; Zech, S. G.; Zhao, J.; Stehlik, D.; Bryant, D. A.; Golbeck, J. H. *J. Biol. Chem.* **2002**, *277*, 20355−20366.
(45) Razeghifard, M. R.; Kim, S.; Patzlaff, J. S.; Hutchison, R. S.; Krick, T.; Ayala, I.; Steenhuis, J. J.; Boesch, S. E.; Wheeler, R. A.; Barry, B. A. *J. Phys. Chem. B* **1999**, *103*, 9790−9800.
(46) Rippka, R.; Derulles, J.; Waterbury, J. B.; Herdman, M.; Stanier, R. *J. Gen. Microbiol.* **1979**, *111*, 1−61.
(47) Barry, B. A. *Methods Enzymol.* **1995**, *258*, 303−319.
(48) Kim, S.; Sacksteder, C. A.; Bixby, K. A.; Barry, B. A. *Biochemistry* **2001**, *40*, 15384−15395.
(49) Parrett, K. G.; Mehari, T.; Warren, P. G.; Golbeck, J. H. *Biochim. Biophys. Acta* **1989**, *973*, 324−332.
(50) Parrett, K. G.; Mehari, T.; Golbeck, J. H. *Biochim. Biophys. Acta* **1990**, *1015*, 341−352.
(51) Warren, P. V.; Golbeck, J. H.; Warden, J. T. *Biochemistry* **1993**, *32*, 849−857.
(52) Piccioni, R.; Bellemare, G.; Chua, N. Methods of Polyacrylamide Gel Electrophoresis in the Analysis and Preparation of Plant Polypeptides. In *Methods in Chloroplast Molecular Biology*; Edelman, H., Hallick, R. B., Chua, N.-H., Eds.; Elsevier: Amsterdam, The Netherlands, 1982; pp 985−1014.
(53) Kruip, J.; Chitnis, P.; Lagoutte, B.; Rögner, M.; Boekema, E. J. *J. Biol. Chem.* **1997**, *272*, 17061−17069.
(54) Kim, S.; Barry, B. A. *J. Am. Chem. Soc.* **2000**, *122*, 4980−4981.
(55) Barry, B. A.; Babcock, G. T. *Proc. Natl. Acad. Sci. U.S.A.* **1987**, *84*, 7099−7103.
(56) Kim, S.; Patzlaff, J.; Krick, T.; Ayala, I.; Sachs, R. K.; Barry, B. A. *J. Phys. Chem. B* **2000**, *104*, 9720−9727.
(57) Patzlaff, J. S.; Barry, B. A. *Biochemistry* **1996**, *35*, 7802−7811.
(58) Kim, S.; Barry, B. A. *Biophys. J.* **1998**, *74*, 2588−2600.
(59) Sacksteder, C. A.; Bender, S. L.; Barry, B. A. *J. Am. Chem. Soc.* **2005**, *127*, 7879−7890.
(60) Becke, A. D. *J. Chem. Phys.* **1993**, *98*, 1372−1377.
(61) Scott, A. P.; Radom, L. *J. Phys. Chem.* **1996**, *100*, 16502−16513.
(62) Slater, J. C. *Quantum Theory of Molecules and Solids*; McGraw-Hill: New York, 1974; Vol. 4.
(63) Becke, A. D. *Phys. Rev. A* **1988**, *38*, 3098−3100.
(64) Vosko, S. H.; Wilk, L.; Nusair, M. *Can. J. Phys.* **1980**, *58*, 1200−1211.
(65) Lee, C.; Yang, W.; Parr, R. G. *Phys. Rev. B* **1988**, *37*, 785−789.
(66) Hehre, W. J.; Radom, L.; Schleyer, P. v. R.; Pople, J. A. *Ab Initio Molecular Orbital Theory*; John Wiley & Sons: New York, 1986.
(67) Helgaker, T.; Taylor, P. R. *Modern Electronic Structure Theory, Part II*; Yarkony, D. R., Ed.; World Scientific: Singapore, 1995; Vol. 2, pp 725−856.
(68) Boesch, S. E.; Wheeler, R. A. *J. Phys. Chem.* **1995**, *99*, 8125−8134.
(69) Boesch, S. E.; Wheeler, R. A. *J. Phys. Chem. A* **1997**, *101*, 8351−8359.
(70) Boesch, S. E.; Wheeler, R. A. *J. Phys. Chem. A* **1997**, *101*, 5799−5804.
(71) Grafton, A. K.; Wheeler, R. A. *J. Comput. Chem.* **1998**, *19*, 1663−1674.
(72) Grafton, A. K.; Wheeler, R. A. *Comput. Phys. Commun.* **1998**, *113*, 78−84.
(73) Wise, K. E.; Grafton, A. K.; Wheeler, R. A. *J. Phys. Chem. A* **1997**, *101*, 1160−1165.
(74) Frisch, M. J.; Trucks, G. W.; Schlegel, H. B.; Scuseria, G. E.; Robb, M. A.; Cheeseman, J. R.; Montgomery, J. A., Jr.; Vreven, T.; Kudin, K. N.; Burant, J. C.; Millam, J. M.; Iyengar, S. S.; Tomasi, J.; Barone, V.; Mennucci, B.; Cossi, M.; Scalmani, G.; Rega, N.; Petersson, G. A.; Nakatsuji, H.; Hada, M.; Ehara, M.; Toyota, K.; Fukuda, R.; Hasegawa, J.; Ishida, M.; Nakajima, T.; Honda, Y.; Kitao, O.; Nakai, H.; Klene, M.; Li, X.; Knox, J. E.; Hratchian, H. P.; Cross, J. B.; Bakken, V.; Adamo, C.; Jaramillo, J.; Gomperts, R.; Stratmann, R. E.; Yazyev, O.; Austin, A. J.; Cammi, R.; Pomelli, C.; Ochterski, J. W.; Ayala, P. Y.; Morokuma, K.; Voth, G. A.; Salvador, P.; Dannenberg, J. J.; Zakrzewski, V. G.; Dapprich, S.; Daniels, A. D.; Strain, M. C.; Farkas, O.; Malick, D. K.; Rabuck, A. D.; Raghavachari, K.; Foresman, J. B.; Ortiz, J. V.; Cui, Q.; Baboul, A. G.; Clifford, S.; Cioslowski, J.; Stefanov, B. B.; Liu, G.; Liashenko, A.; Piskorz, P.; Komaromi, I.; Martin, R. L.; Fox, D. J.; Keith, T.; Al-Laham, M. A.; Peng, C. Y.; Nanayakkara, A.; Challacombe, M.; Gill, P. M. W.; Johnson, B.; Chen, W.; Wong, M. W.; Gonzalez, C.; Pople, J. A. *Gaussian 03*, revision D.01; Gaussian, Inc.: Wallingford, CT, 2004.
(75) Schlegel, H. B. *J. Comput. Chem.* **1982**, *3*, 214−218.
(76) Wasikowski, C.; Klemm, S. *XMOL*, version 1.3.1; Research Equipment, Inc. d.b.a. Minnesota Supercomputer Center, Inc., 1993.
(77) Wise, K. E.; Pate, J. B.; Wheeler, R. A. *J. Phys. Chem. B* **1999**, *103*, 4764−4772.
(78) York, S. S.; Boesch, S. E.; Wheeler, R. A.; Frech, R. *Macromolecules* **2003**, *36*, 7348−7351.
(79) Golbeck, J. H. *In The Molecular Biology of Cyanobacteria*; Kluwer Academic Publishers: Dordrecht, The Netherlands, 1994; Vol. 1, pp 319−360.
(80) Brettel, K.; Leibl, W. *Biochim. Biophys. Acta* **2001**, *1507*, 100−114.
(81) Shen, G.; Zhao, J.; Reimer, S. K.; Antonkine, M. L.; Cai, Q.; Weiland, S. M.; Golbeck, J. H.; Bryant, D. A. *J. Biol. Chem.* **2002**, *277*, 20343−20354.
(82) Vassiliev, I. R.; Jung, Y.-S.; Mamedov, M. D.; Semenov, A. Y.; Golbeck, J. H. *Biophys. J.* **1997**, *72*, 301−315.
(83) Brettel, K.; Golbeck, J. H. *Photosynth. Res.* **1995**, *45*, 183−193.
(84) Breton, J.; Nabedryk, E.; Leibl, W. *Biochemistry* **1999**, *38*, 11585−11592.
(85) Bauscher, M.; Maentele, W. *J. Phys. Chem.* **1992**, *96*, 11101−11108.
(86) Breton, J.; Burie, J.-R.; Berthomieu, C.; Berger, G.; Nabedryk, E. *Biochemistry* **1994**, *33*, 4953−4965.
(87) Breton, J. *Proc. Natl. Acad. Sci. U.S.A.* **1997**, *94*, 11318−11323.
(88) Grotjohann, I.; Fromme, P. *Photosynth. Res.* **2005**, *85*, 51−72.
(89) Pushkar, Y. N.; Ayzatulin, O.; Stehlik, D. *Appl. Magn. Res.* **2005**, *28*, 195−211.
(90) Hanley, J.; Deligiannakis, Y.; MacMillan, F.; Bottin, H.; Rutherford, A. W. *Biochemistry* **1997**, *36*, 11543−11549.
(91) van der Est, A.; Prisner, T.; Bittl, R.; Fromme, P.; Lubitz, W.; Moebius, K.; Stehlik, D. *J. Phys. Chem. B* **1997**, *101*, 1437−1443.
(92) MacMillan, F.; Hanley, J.; van der Weerd, L.; Knupling, M.; Un, S.; Rutherford, A. W. *Biochemistry* **1997**, *36*, 9297−9303.
(93) Kaupp, M. *Biochemistry* **2002**, *41*, 2895−2900.
(94) Suydam, I. T.; Boxer, S. G. *Biochemistry* **2003**, *42*, 12050−12055.
(95) Plokhotnichenko, A. M.; Radechenko, E. D.; Stepanian, S. G.; Adamowicz, L. *Recent Res. Devel. Phys. Chem.* **1998**, *2*, 1087−1104.
(96) Hermansson, K. *J. Phys. Chem. A* **2002**, *106*, 4695−4702.
(97) Hobza, P.; Havlas, Z. *Chem. Rev.* **2000**, *100*, 4253−4264.
(98) McCarthy, W.; Smets, J.; Adamowicz, L.; Plokhotnichenko, A. M.; Radechenko, E. D.; Sheina, G. G.; Stepanian, S. G. *Mol. Phys.* **1997**, *91*, 513−525.
(99) Saeki, M.; Akagi, H.; Fujii, M. *J. Chem. Theory Comput.* **2006**, *2*, 1176−1183.
(100) Lee, C.; Park, K. H.; Cho, M. *J. Chem. Phys.* **2006**, *125*, 114508/1−114508/16.
(101) Miles, H. T.; Frazier, J. *Biochemistry* **1978**, *17*, 2920−2927.
(102) Liquier, J.; Taillandier, E. *Infrared Spectroscopy of Biomolecules*; Manstch, H. H., Chapman, D., Eds.; Wiley-Liss: New York, 1996; pp 131−158.
(103) Maevsky, A. A.; Sukhorukov, B. I. *Nucleic Acids Res.* **1980**, *8*, 3029−3042.